5

Electromagnetic Waves in Cavity Design

Hyoung Suk Kim
Kyungpook National University
Korea

1. Introduction

Understanding electromagnetic wave phenomena is very important to be able to design RF cavities such as for atmospheric microwave plasma torch, microwave vacuum oscillator/amplifier, and charged-particle accelerator. This chapter deals with some electromagnetic wave equations to show applications to develop the analytic design formula for the cavity. For the initial and crude design parameter, equivalent circuit approximation of radial line cavity has been used. The properties of resonator, resonant frequency, quality factor, and the parallel-electrodes gap distance have been considered as design parameters. The rectangular cavity is introduced for atmospheric microwave plasma torch as a rectangular example, which has uniform electromagnetic wave distribution to produce wide area plasma in atmospheric pressure environment. The annular cavity for klystrode is introduced for a microwave vacuum oscillator as a circular example, which adapted the grid structure and the electron beam as an annular shape which gives high efficiency compared with conventional klystrode. Some simulation result using the commercial software such as HFSS and MAGIC is also introduced for the comparison with the analytical results.

2. Equivalent circuit approximation of radial-line cavity

Microwave circuits are built of resonators connected by waveguides and coaxial lines rather than of coils and condensers. Radiation losses are eliminated by the use of such closed elements and ohmic loss is reduced because of the large surface areas that are provided for the surface currents. Radio-frequency energy is stored in the resonator fields. The linear dimensions of the usual resonator are of the order of magnitude of the free-space wavelength corresponding to the frequency of excitation. A simple cavity completely enclosed by metallic walls can oscillate in any one of an infinite number of field configurations. The free oscillations are characterized by an infinite number of resonant frequencies corresponding to specific field patterns of modes of oscillation. Among these frequencies there is a smallest one,

$$f_0 = c/\lambda_0 \tag{1}$$

, where the free-space wavelength is of the order of magnitude of the linear dimensions of the cavity, and the field pattern is unusually simple; for instance, there are no internal nodes in the electric field and only one surface node in the magnetic field.

The oscillations of such a cavity are damped by energy lost to the walls in the form of heat. This heat comes from the currents circulating in the walls and is due to the finite conductivity of the metal of the walls. The total energy of the oscillations is the integral over the volume of the cavity of the energy density,

$$W = \frac{1}{2}\int_v \left(\varepsilon_0 E^2 + \mu_0 H^2\right) dv \tag{2}$$

$$\mu_0 = 4\pi \times 10^{-7}\, H/m \text{ and } \varepsilon_0 = \frac{1}{36\pi} \times 10^{-9}\, F/m \tag{3}$$

, where E and H are the electric and magnetic field vectors, in volts/meter and ampere-turns/meter, respectively. The cavity has been assumed to be empty. The total energy W in a particular mode decreases exponentially in time according to the expression,

$$W = W_0 e^{-\frac{\omega_0 t}{Q}} \tag{4}$$

, where $\omega_0 = 2\pi f_0$ and Q is a quality factor of the mode which is defined by

$$Q = \frac{2\pi(\textit{energy stored in the cavity})}{(\textit{energy lost in one cycle})}. \tag{5}$$

The fields and currents decrease in time with the factor $e^{-\frac{\omega_0 t}{Q}}$.
Most klystrons and klystrodes are built with cavities of radial-line types. Several types of reentrant cavities are shown in Fig. 1. It is possible to give for the type of cylindrical reentrant cavities a crude but instructive mathematical description in terms of approximate solutions of Maxwell's equations.

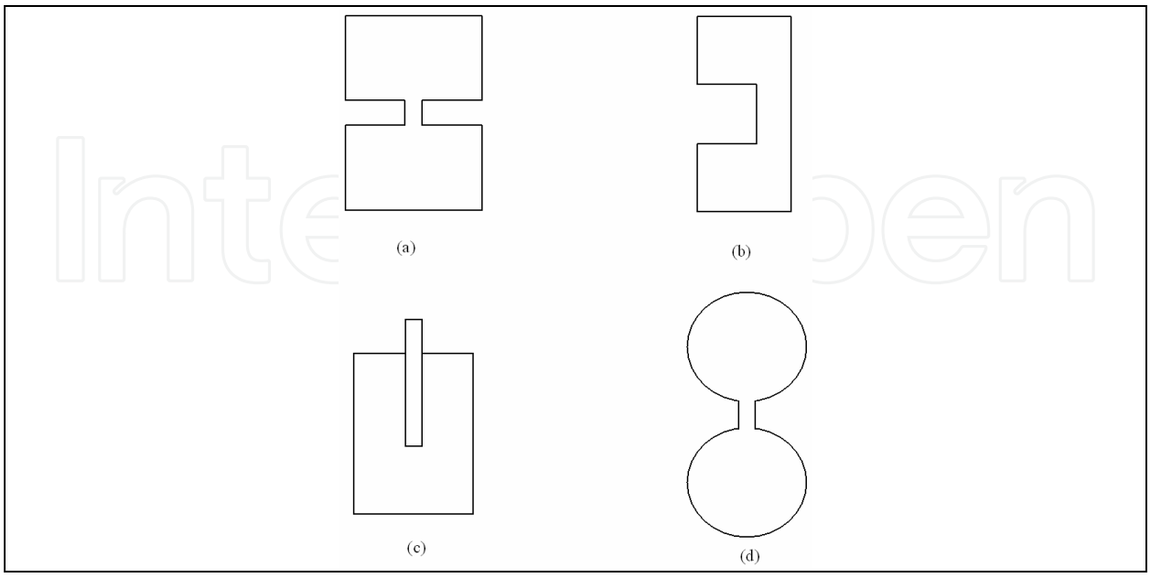

Fig. 1. Resonant cavities; (a) Coaxial cavity, (b) Radial cavity, (c) Tunable cavity,
(d) Toroidal cavity

The principle, or fundamental, mode of oscillation of such cavity, and the one with the longest free-space wavelength , has electric and magnetic fields that do not depend on the azimuthal angle defining the half plane though both the axis and the point at which the fields are being considered. In addition, the electric field is zero only at wall farthest apart from the gap and the magnetic field is zero only at the gap. In this mode the magnetic field is everywhere perpendicular to the plane passing through the axis the electric field lies in that plane. Lines of magnetic flux form circles about the axis and lines of electric flux pass from the inner to the outer surfaces.

In the principle mode of radial-line cavity only E_z , and H_z are different from zero and these quantities are independent of ϕ . (see Fig. 2 for cylindrical coordinates and dimensions of the cavity). The magnetic field automatically satisfies the conditions of having no normal component at the walls.

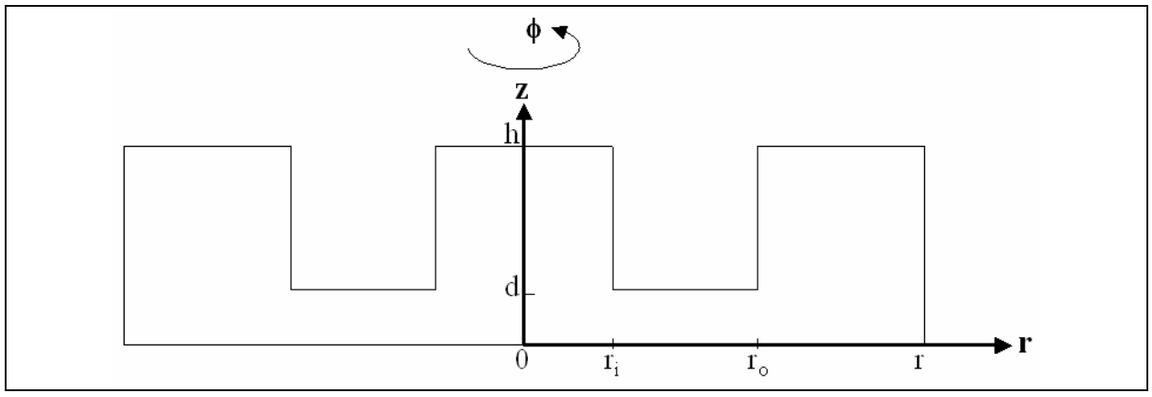

Fig. 2. Cylindrical coordinates and dimensions of the radial cavity

The cavities in which RF interaction phenomena happens with charged particles almost always have a narrow gap, that is, the depth of the gap d (see Fig. 2), is small compared with the radius r_0 of the post ($d \langle\langle r_0$ in Fig. 2).. If the radius of the post is much less than one-quarter of the wavelength, and if the rest of the cavity is not small, the electric field in the gap is relatively strong and approximately uniform over the gap. It is directed parallel to the axis and falls off only slightly as the edge of the gap is approached. On the other hand, the magnetic field increases from zero at the center of the gap in such a manner that it is nearly linear with the radius.

In a radial-line cavity the electric field outside the gap tends to remain parallel to the axis, aside from some distortion of the field that is caused by fringing near the gap; it is weaker than in the gap and tends to become zero as the outer circular wall is approached. The magnetic field, on the other hand, increases from its value at the edge of the gap and has its maximum value at the outer circular wall.

It is seen that, whereas the gap is a region of very large electric field and small magnetic field, the reentrant portion of the cavity is a region of large magnetic field and small electric field. The gap is the capacitive region of the circuit, and the reenetrant portion is the inductive region. Charge flows from the inner to the outer conducting surface of the gap by passing along the inner wall, across the outer end. The current links the magnetic flux and the magnetic flux links the current, as required by the laws of Faraday, Biot and Savart.

2.1 Capacitance in cylindrical cavity

If the gap is narrow, the electric field in the gap is practically space-constant. Thus the electric field E_z in the gap of the circular cavity (see Fig. 2) comes from Gauss' law,

$$E_z = \frac{\sigma}{\varepsilon_0} = \frac{Q}{\varepsilon_0 \pi (r_0^2 - r_i^2)} . \tag{6}$$

At the end of the cavity near to the gap both E_z and E_r exist and the field equations are more complicated. If d is small compared with h and r, it can be assumed that the fields in the gap are given approximately by the preceding equation.
Therefore,

$$C = \frac{Q}{V} = \frac{Q}{E_z d} = \frac{\varepsilon_0 \pi (r_0^2 - r_i^2)}{d} . \tag{7}$$

2.2 Inductance in cylindrical cavity

The magnetic field H_φ comes from Ampere's law,

$$\oint H r d\theta = I . \tag{8}$$

Therefore,

$$B = \frac{\mu_0 I}{2\pi r} . \tag{9}$$

The total magnetic flux in the cylindrical cavity,

$$\Phi = \int_{r_0}^{r} B h dr = \frac{\mu_0 I h}{2\pi} \int_{r_0}^{r} \frac{dr}{r} = \frac{\mu_0 I h}{2\pi} \ln \frac{r}{r_0} . \tag{10}$$

Comparing this with inductance definition, $\Phi = LI$, we get the followings;

$$L = \frac{\mu_0}{2\pi} h \ln \frac{r}{r_0} . \tag{11}$$

2.3 Resonance frequency in cylindrical cavity

The resonant wavelength of a particular mode is found from a proper solution of Maxwell's equation, that is, one that satisfies the boundary conditions imposed by the cavity. When the walls of the cavity conduct perfectly, these conditions are that the electric field must be perpendicular to the walls and the magnetic field parallel to the walls over the entire surface, where these fields are not zero.
The resonant frequency f_0 could be calculated for the principal mode of the simple reentrant cavity. The resonant cavity is modeled by parallel LC circuits as can be seen in Fig. 3. In fact, cavities are modeled as parallel resonant LC circuits in order to facilitate discussions or analyses. The resonant frequency is inversely proportional to the square root of inductance and capacitance;

$$\omega = \frac{1}{\sqrt{LC}} = \frac{1}{\sqrt{\frac{\varepsilon_0 \mu_0}{2} \frac{r_0^2 - r_i^2}{d} h \ln \frac{r}{r_0}}}. \tag{12}$$

2.4 Unloaded Q in cylindrical cavity

In the cavity undergoing free oscillations, the fields and surface currents all vary linearly with the degree of excitation, that is, a change in one quantity is accompanied by a proportional change in the others. The stored energy and the energy losses to the walls vary quadratically with the degree of excitation.

Since the quality factor Q of the resonator is the ratio of the stored energy and the energy losses per cycle to the walls, it is independent of the degree of excitation.

$$Q = \frac{2\pi f(energy\ stored\ in\ the\ cavity)}{(power\ lost)} = \omega_0 \frac{U}{P_{loss}} = \omega \frac{\frac{1}{2} LI^2}{\frac{1}{2} RI^2} = \omega \frac{L}{R}. \tag{13}$$

The resonator losses per second, besides being proportional to the degree of excitation, are inversely proportional to the product of the effective depth of penetration of the fields and currents into the walls, the skin depth, and the conductivity of the metal of the walls. Since the skin depth is itself inversely proportional to the square root of the conductivity, the losses are inversely proportional to the square root of the conductivity. The losses are also roughly proportional to the total internal surface area of the cavity; and this area is proportional to the square of the resonant wavelength for geometrically similar resonators. The skin depth is proportional to the square root of the wavelength, and hence the losses per second are proportional to the three-halves power of the resonant wavelength.

The loss per cycle, which is the quantity that enters in Q, is proportional to the five-halves power of the resonant wavelength. Since the energy stored is roughly proportional to the volume, or the cube of the wavelength, the Q varies as the square root of the wavelength for geometrically similar cavities, a relationship that is exact if the mode is unchanged because the field patterns are the same. In general, large cavities, which have large resonant wavelengths in the principal mode, have large values of Q. Cavities that have a surface area that is unusually high in proportion to the volume, such as reentrant cavities, have Q's that are lower than those of cavities having a simpler geometry.

The surface current, J, is equal in magnitude to H_ϕ at the wall. The power lost is the surface integral over the interior walls of the cavity.

$$\begin{aligned} P_{loss} &= \frac{R_s}{2} \int J^2 ds = \frac{R_s}{2} \int |H_\phi|^2 \, ds \\ &= \frac{R_s}{2} \left[\left(\frac{I}{2\pi r_o} \right)^2 2\pi r_0 (h-d) + 2 \int_{r_0}^{r} \left(\frac{I}{2\pi r_0} \right)^2 2\pi r dr + \left(\frac{I}{2\pi r_o} \right)^2 2\pi r h \right] \\ &= \frac{R_s I^2}{2\pi} \left[\frac{h-d}{r_0} + 2 \ln \frac{r}{r_0} + \frac{h}{r} \right] \equiv \frac{1}{2} RI^2, \end{aligned} \tag{14}$$

where the shunt resistance is

$$R \equiv \frac{R_s}{2\pi}\left[\frac{h-d}{r_0} + 2\ln\frac{r}{r_0} + \frac{h}{r}\right]. \tag{15}$$

The surface current can be considered concentrated in a layer of resistive material of thickness. Surface resistance is that

$$R_s = \frac{1}{\sigma\delta} = \frac{1}{\sigma\sqrt{\frac{1}{\pi f \mu\sigma}}} = \sqrt{\frac{\pi f \mu}{\sigma}}. \tag{16}$$

As an example, the conductivity of copper is $\sigma_{copper} = 5.8\times10^7 / \Omega m$ and since copper is nonmagnetic $\mu_{copper} = \mu_0 = 4\pi\times10^{-7} H/m$, hence, in case of that cavity material is copper, for f=6GHz,

$$\begin{aligned} &\delta = 0.85\mu m \\ &R_s = 2.02\times10^{-2}\Omega \\ &R = 2.66\times10^{-3}\Omega \\ &L = 1.01\times10^{-10} H \\ &Q_0 = \omega\frac{L}{R} = 1431. \end{aligned} \tag{17}$$

The shunt conductance G is, as given by the expression,

$$G = \frac{(energy\ lost\ per\ \mathrm{sec}ond)}{V(t)^2} \tag{18}$$

is defined only when the voltage $V(t)$ is specified. In a reentrant cavity the potential across the gap varies only slightly over the gap if the gap is narrow and the rest of the cavity is not small. A unique definition is obtained for G by using for $V(t)$ the potential across the center of the gap. The gap voltage is proportional to the degree of excitation, and hence the shunt conductance is independent of the degree of excitation. For geometrically similar cavities the shunt conductance varies inversely as the square root of the resonant wavelength for the same mode of excitation. This relationship exists because for the same excitation $V(t)^2$ is proportional to the square of the wavelength and the loss per second to the three-halves power of the wavelength.

2.5 Lumped-constant circuit representation

The main value of the analogy between resonators and lumped-constant circuits lies not in the extension of characteristic parameters to other geometries, in which the analogy is not very reliable, but in the fact that the equations for the forced excitation of resonators and lumped-constant circuits are of the same general form.

If, for example, it is assumed that the current i(t) passes into the shunt combination of L, C and conductance G, by Kirchhoff's laws, (see Fig. 3)

$$i(t) = C\frac{dV(t)}{dt} + \frac{1}{L}\int V(t)dt + GV(t). \tag{19}$$

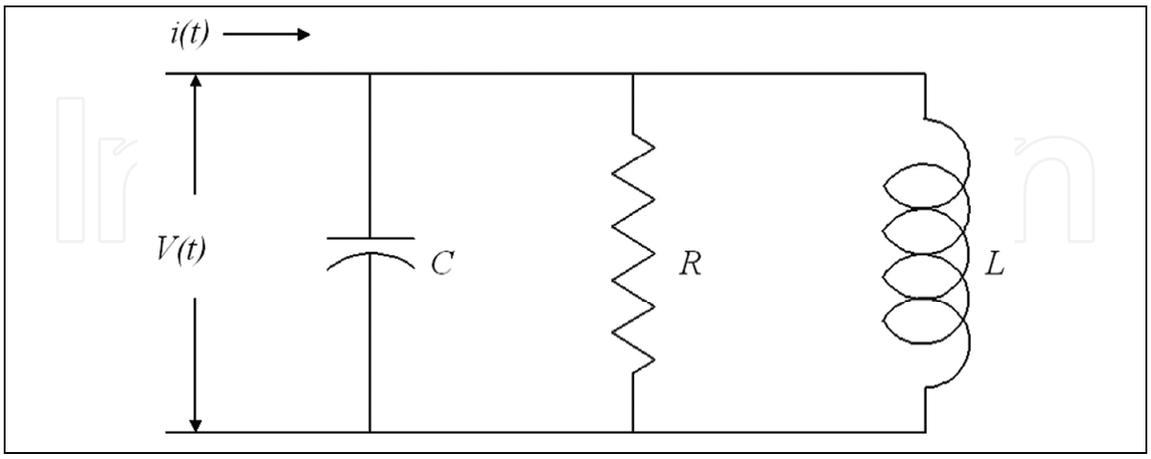

Fig. 3. Limped-constant circuit

On taking the derivative and eliminating L,

$$\frac{di(t)}{dt} = C\left[\frac{d^2V(t)}{dt^2} + \omega_0^2 V(t)\right] + G\frac{V(t)}{dt}. \tag{20}$$

In other word,

$$\frac{\omega}{C}\frac{di(t)}{d\theta} = \omega^2\frac{d^2V(t)}{d\theta^2} + 2\gamma\omega\frac{dV(t)}{d\theta} + \omega_0^2 V(t), \tag{21}$$

where $\gamma = G/2C$, $\omega_0 = 1/\sqrt{LC}$ and $\theta = \omega t$, which are used to calculate numerically the initial beam effect in the last chapter.
For a forced oscillation with the frequency ω,

$$i_\omega = \left[G + j\omega_0 C\left(\frac{\omega}{\omega_0} - \frac{\omega_0}{\omega}\right)\right]V_\omega. \tag{22}$$

Thus, there is defined circuit admittance

$$Y = G + j\omega_0 C\left(\frac{\omega}{\omega_0} - \frac{\omega_0}{\omega}\right). \tag{23}$$

These equations describe the excitation of the lumped-constant circuit.

3. Numerical analysis for the high frequency oscillator system with cylindrical cavity

In this section, we will meet an circular cavity example of a klystrode as a high frequency oscillator system with the knowledge which is described in previous sections.

Conventional klystrodes and klystrons often have toroidal resonators, i.e., reentrant cavity with a loop or rod output coupler for power extraction. These resonators commonly use solid-electron-beam which could limit the output power. One way to get away this limitation is to use the annular beam as was commonly done in TWTs. The main reason using reentrant cavities in most microwave tubes with circular cross sections is that the gap region should produce high electric field and thus high interaction impedance of the electron beam when the cavity is excited. In our design we assume a short cavity length, d, along the longitudinal direction parallel to the electron motion. In the meantime the width of electron beam tunnel, $r_0 - r_i$, is much larger, i.e. $d \langle\langle r_0 - r_i$ as shown in Fig 4. And thus the efficiency of beam and RF interaction in this klystrode cavity depends sensitively upon the cavity shape at the beam entrance of the RF cavity in the beam tunnel. A simple trade-off study suggests to put to use of gridded plane, so-called a cavity grid (anode), so that the eigenmode of the reentrant cavity is maintained. With the gridded plane removed and left open, the TM01-mode has many competing modes and the interaction efficiency disappears. The use of thin cavity grid in the beam tunnel, however, can slightly reduce the electron beam transmission, which will not pose a much of problem when the same type of grid is used in between the cathode and anodic cavity grid. In the simulations with the MAGIC and HFSS codes, the anodic cavity grid could be assumed to be a smooth conducting surface, and pre-bunched electrons were launched from those surfaces of cavity grid. This kind of concept can provide a compact microwave source of low cost and high efficiency that is of strong interest for industrial, home electronics and communications applications.

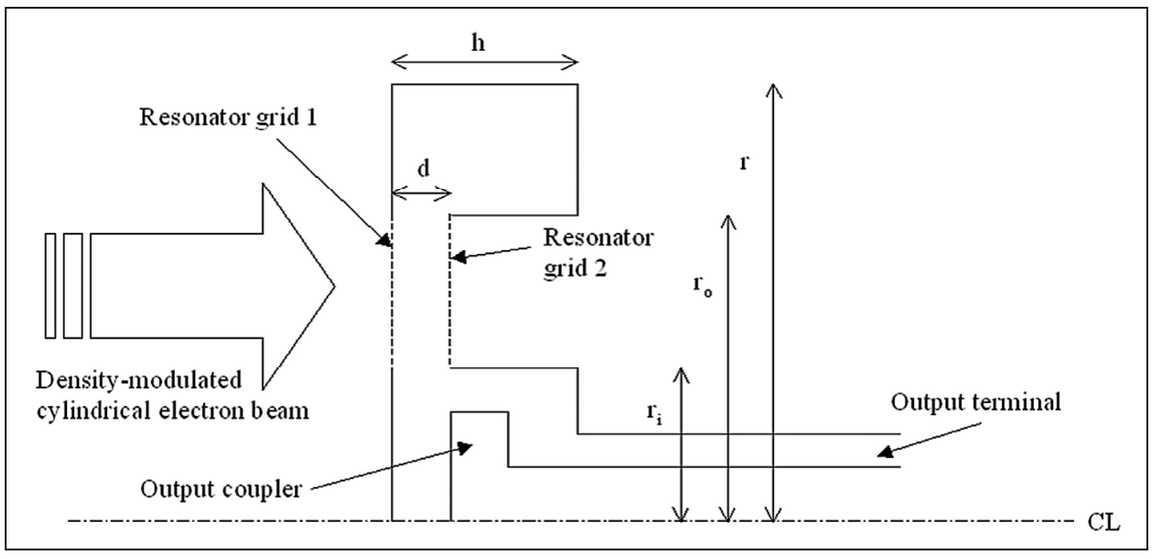

Fig. 4. Schematics of the annular beam klystrode with the resonator grids for the high electric field and high interaction efficiency in the gap region. This cavity structure allows easier power extraction through the center coax coupler

The klystrodes consist of the gated triode electron gun, the resonator and the collector. The gated electron gun provides with the pre-modulated electron bunches at the fundamental frequency of the input resonator, where the voltage on the grid electrode is controlled by an external oscillator or feedback system. The other possible type of gated electron guns could

be the field-emitter-array gun, RF gun, and photocathode. The electron bunches arrive at the output gap with constant kinetic energy but with the density pre-modulated. Here, we assumed the electron beam is operated on class B operation, that is, electron bunch length is equal to one half of the RF period. Through the interaction between electron beam and RF field, the kinetic energy is extracted from the pre-modulated electrons and converted into RF energy.

Figure 4 shows the schematics of the circular gridded resonator with center coupling mechanism for the easy and efficient power extraction. In this section, we will describe the design of annular beam klystrode in C-band.

3.1 RF interaction cavity design

As we have seen in previous section, using the lumped-circuit approach, the resonant frequency of this protuberance cavity with the annular beam is expressed as

$$\omega = \frac{1}{LC} = \frac{1}{\sqrt{\frac{\varepsilon_0 \mu_0}{2} \frac{r_0^2 - r_i^2}{d} h \ln \frac{r}{r_0}}}. \tag{24}$$

Since this expression is an approximation which gives the tendency of frequency variation when we are adjusting design parameters, we can perform parameter tuning exercise using design tools such as HFSS. Fig. 5 shows an example of the detailed design using HFSS where the emission was introduced at the gap region between inner radial distances of 5.7 and 9.4mm. In the figure, the electric field is enhanced and fairly uniform due to the presence of resonator grid1 and resonator grid2. The grid structure in beam inlet and beam outlet make the electric field maintain fairly high intensity in the gap region through which the electron beam passes to interact with RF. Figure 6 also show scattering parameter plots where resonator grids of the klystrode are considered closed metal wall and the cavity has only output terminal as one port system. The bold line is the real value of S and the thin line is the imaginary one. The resonator frequency is 5.78 GHz in the absence of finite conductivity of cavity and electron beam.

The detailed tuning of beam parameters for efficient klystrode could be investigated using PIC code such as MAGIC. As an example, the current is assumed density-modulated in the input cavity and cut-off sinusoidal,

$$\begin{aligned} I(z=0,t) &= I_0 MAX\left(\sin(\omega t), 0\right) \\ &= I_0 \left[\frac{1}{\pi} + \frac{1}{2}\sin(\omega t) - \sum_{n-0}^{\infty} \frac{2}{\pi(4n^2-1)} \cos(2n\omega t)\right] \end{aligned} \tag{25}$$

whose peak current, I_{peak}, is 3 amperes.

The tube is supposed of being operated in class B as shown in Fig. 7. A class B amplifier is one in which the grid bias is approximately equal to the cut-off value of the tube, so that the plate current is approximately zero when no exciting grid potential is applied, and such that plate current flows for approximately one-half of each cycle when an AC grid voltage is applied.

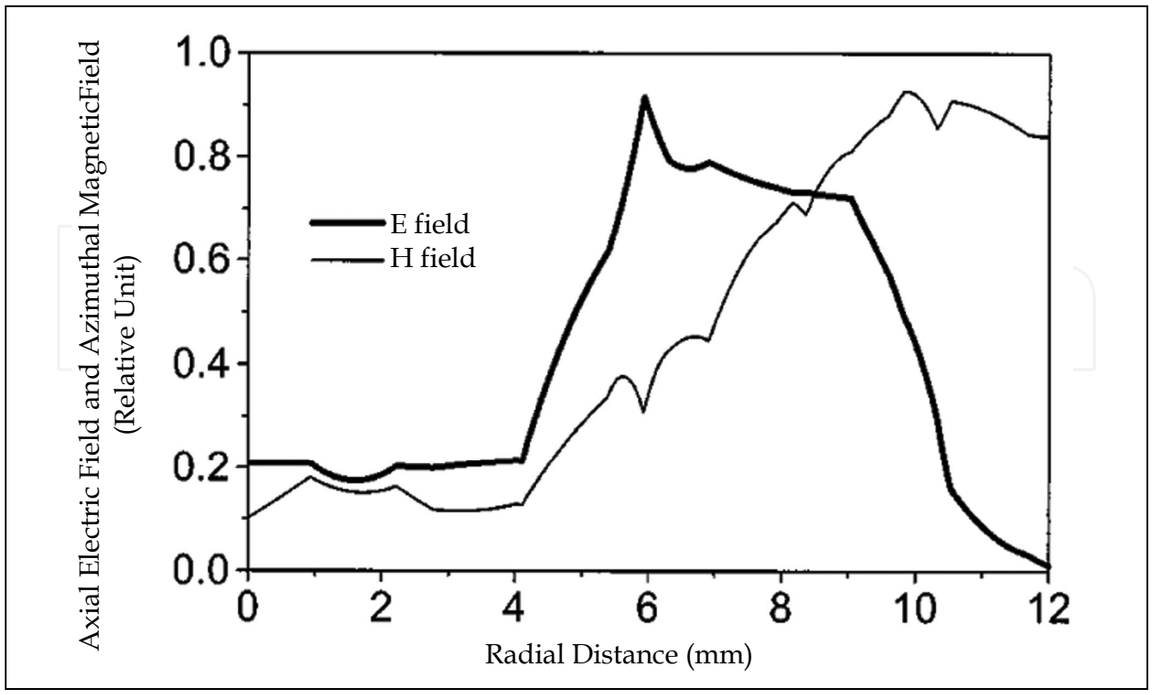

Fig. 5. Magnitude of axial electric field and azimuthal magnetic field (in relative unit) along the radial distance on the mid-plane between resonator grid 1 and grid 2 in the cavity. Emission surface is between the radial distances of 5.7 and 9.4 mm

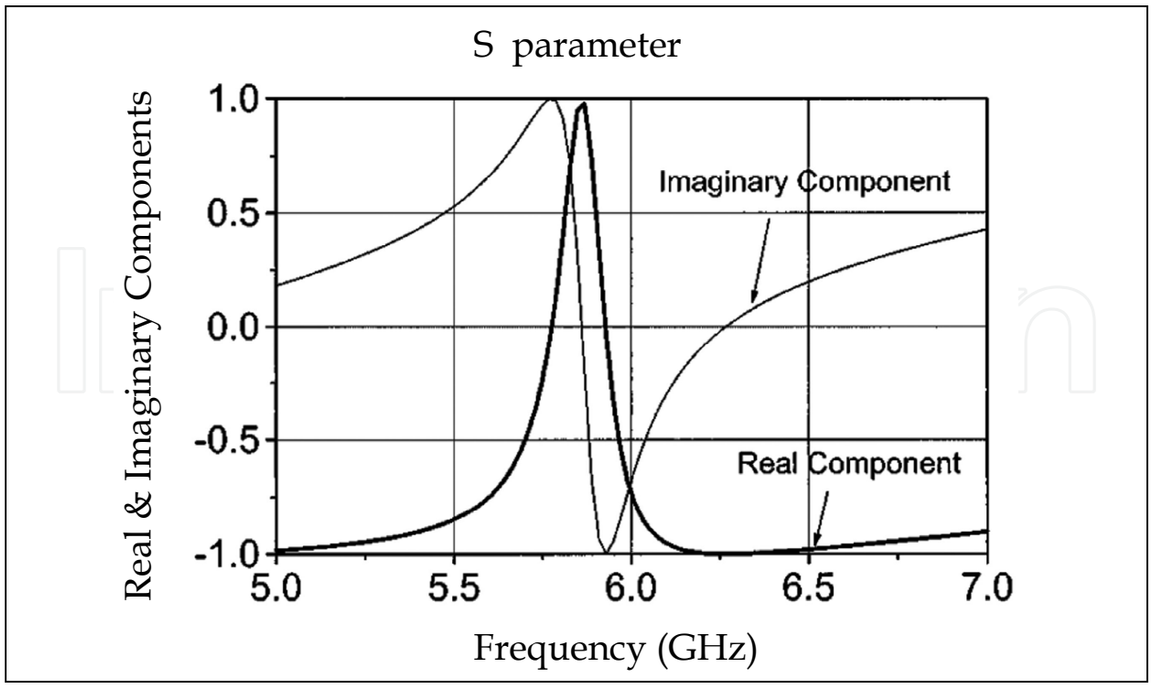

Fig. 6. Scattering parameter plots. The resonator frequency is 5.78 GHz in the absence of finite conductivity of cavity and electron beam

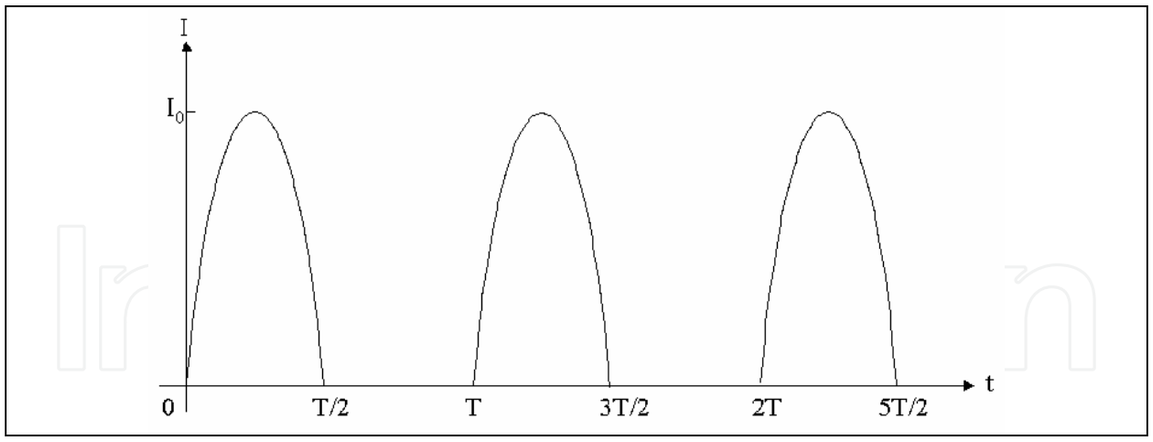

Fig. 7. Pre-modulated electron beam in current vs. time; cut-off sinusoidal current which is used in class B operation, $I = I_0 MAX\left(\sin\left(\omega t\right), 0\right)$

The fundamental mode (TM_{01}-mode) to be interacted with longitudinal traversing electron beam was adapted to our annular beam resonators for the high efficiency device.
Electron transit angle between electrodes gives limitation in the application of the conventional tubes at microwave frequencies. The electron transit angle is defined as

$$\beta = \omega\tau_g = \omega d / v_0 \,, \tag{26}$$

where $\tau_g = d/v_0$ is the transit time across the gap, d is separation between cathode and grid, $v_0 = \sqrt{2eV_0/m} = 0.593\times10^6\sqrt{V_0}$ is the velocity of the electron, and V_0 is DC voltage.

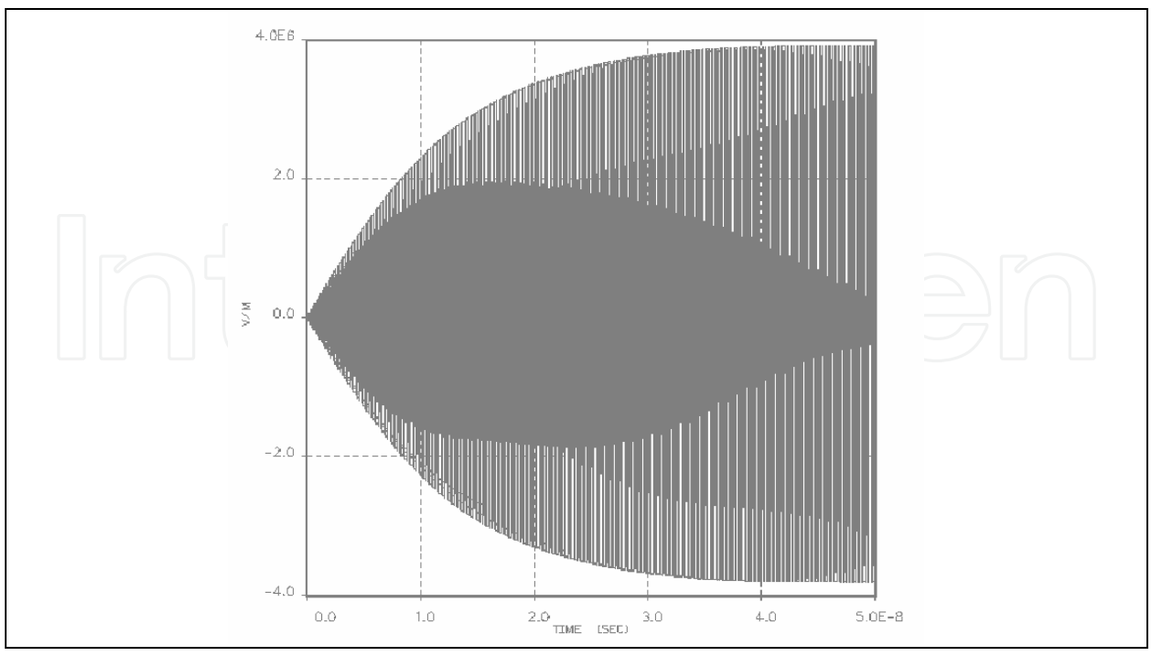

Fig. 8. Electric field in the gap region across the anode electrode 1(grid1) and electrode 2(grid2); The field reaches 4,000,000 V/m

The transit angle was chosen to give that the transit time is much smaller than the period of oscillation for the efficient interaction between RF and electron beam, so that, the beam coupling coefficient, M, is 0.987. The resonant frequency is 5.78 GHz in cold cavity and 6.0 GHz in hot cavity. Although the frequency shift may be greater than the value of normal case, this would be come from the fact that this annular beam covers much more area with electron beam than the conventional solid beam in a given geometry. As we can see in Fig. 8 and Fig. 9, this resonant cavity is filled and saturated with the RF power in 50 ns, and reveals high efficiency of about 67%. The output power is 1250 W so that the efficiency of this annular beam klystrode reveals 67 % at 6.004 GHz.

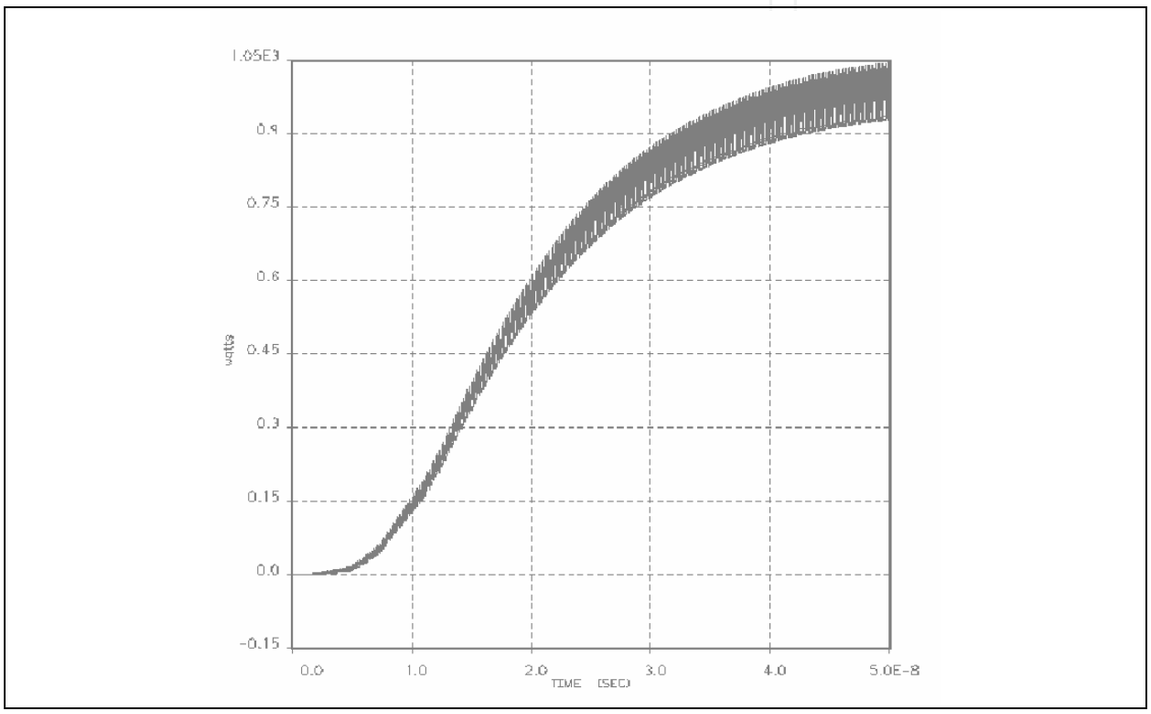

Fig. 9. Output power going through the output port vs. time where driving frequency is 6GHz. It goes to about 1.25kW

3.2 RF interaction efficiency calculation

There are some computational design codes for the klystrode. But in this section, 1-dimensional but realistic electron beam and electric field shape are introduced to develop analytical calculations for the klystrode design, which results in easy formulas for the efficiency and electric field in the gap region of the klystrode in steady state.
Maxwell's equations for electron beams are followings,

$$\nabla \cdot E = -\frac{\rho}{\varepsilon}, \tag{27}$$

$$\nabla \times E = -\frac{\partial B}{\partial t} \tag{28}$$

and

$$\nabla \times H = J + \frac{\partial D}{\partial t}. \tag{29}$$

As an approximation, the electron dynamics is in 1-D space. Then, the Maxwell's equations are simplified as the followings.

$$\frac{\partial E}{\partial z} = -\frac{\rho}{\varepsilon}, \tag{30}$$

$$\frac{\partial B}{\partial t} = 0 \tag{31}$$

and

$$-\rho v + \varepsilon \frac{\partial B}{\partial t} = \varepsilon \frac{\partial E}{\partial z} v + \varepsilon \frac{\partial E}{\partial t} = \varepsilon \frac{dE}{dt} = 0. \tag{32}$$

Therefore, this means that E remains constant for each electrons moving with velocity, v. From the Lorentz force equation,

$$\frac{dv}{dt} = -\frac{e}{m} E = (const.) \tag{33}$$

for each particle with velocity v.
Define the snapshot time be τ such that,

$$\tau = t_x + t_y, \tag{34}$$

where t_x is transit time for the moving particle from resonator grid1 to the transit distance, z, and t_y is leaving time for moving particle from the resonator grid1. Its definition is shown in schematic representation for the transit time, departure time, snapshot time, and transit distance in Fig. 10.
Therefore, we can say that the variables of electrons are denoted by

$$v = v_0 - \frac{e}{m} E(t_y) t_x, \tag{35}$$

$$z = v_0 t_x - \frac{e}{2m} E(t_y) t_x^2 \tag{36}$$

and

$$\rho = \frac{J_{peak}}{v} Max\left(\sin(\omega t_y), 0\right). \tag{37}$$

Let's assume that $E(t_y) = E_0 \sin(\omega t_y)$ which is synchronous to current modulation for the maximum interaction between electron beam and RF-field.

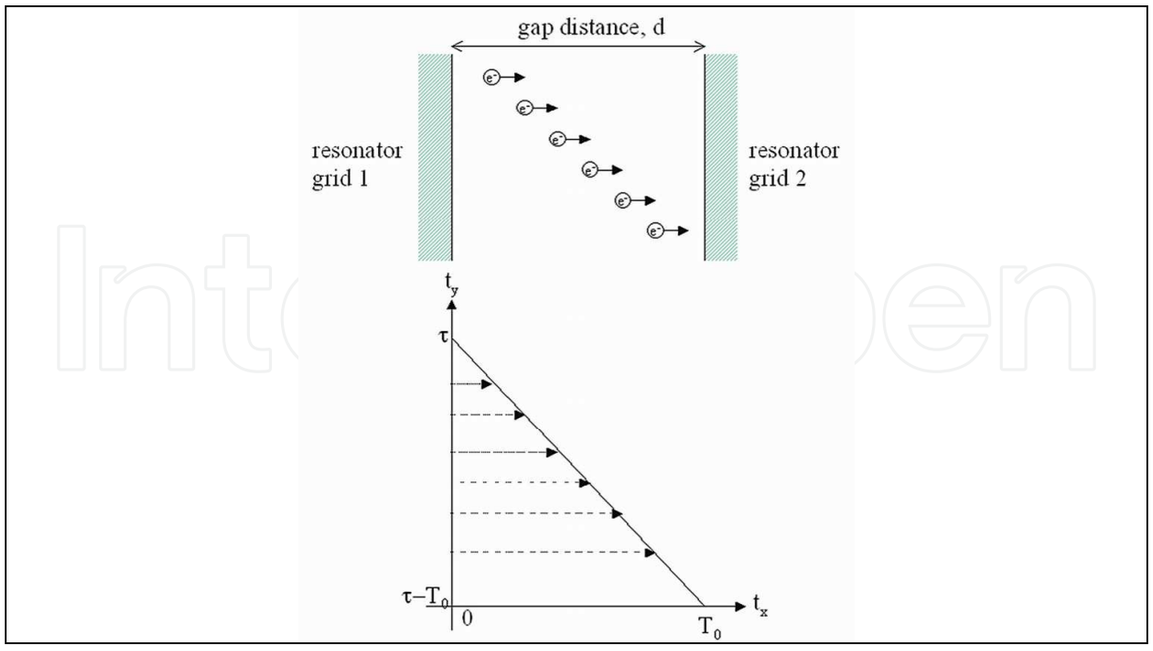

Fig. 10. Schematic representation for the definition of snapshot time (τ), transit time (t_x) to z , departure time (t_y)

Then, we have

$$v = v_0 - \frac{e}{m} E_0 \sin(\omega t_y) t_x \tag{38}$$

and

$$z = v_0 t_x - \frac{e}{2m} E \sin(\omega t_y) t_x^2. \tag{39}$$

By the way, from the above equation,

$$z = \frac{v_0 + v_z}{2} t_x \tag{40}$$

and

$$T = \frac{2d}{v_0 + v_d} \tag{41}$$

so that for $(period) = 167ps(\lambda = 5cm)$

$$T_0 \in [15ps, 30ps], \ \tau \in [0ps, 167ps], \tag{42}$$

and

$$t_x \in [0ps, 30ps]. \tag{43}$$

Figure 11 shows a typical case that electrons are decelerated due to the interaction between RF and electron beam. Extreme case would be 100 % donation of its kinetic energy to RF, which makes its velocity be zero at the resonator grid2. In that case electrons are delayed by 30 ps to the phase of RF field, where the half period of RF is 84 ps (6 GHz).

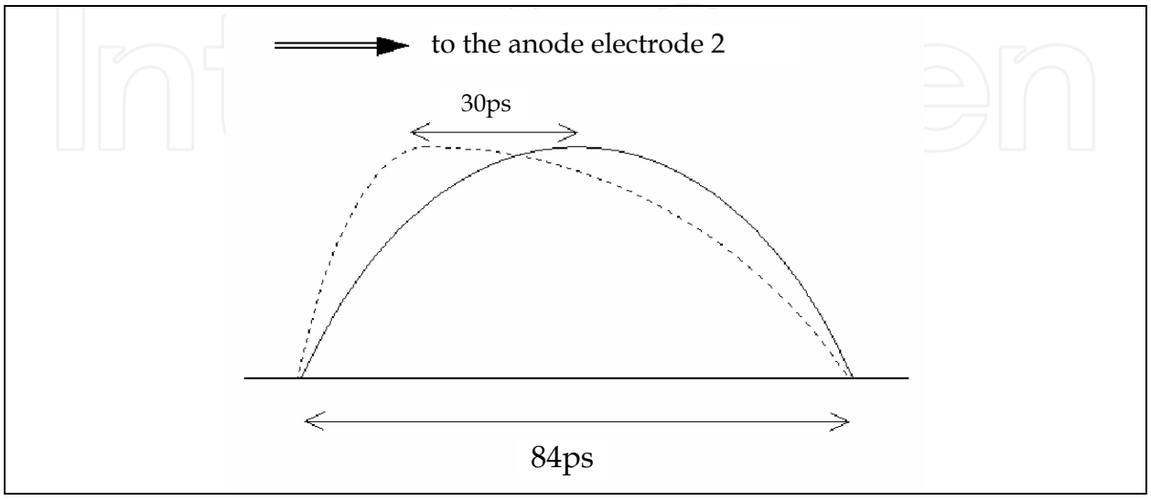

Fig. 11. Electrons are decelerated due to the interaction between RF and electron beam. Extreme case would be 100% donation of its kinetic energy to RF, which makes its velocity be zero at the resonator grid2. In that case electrons are delayed by 30ps to the phase of RF field, where the half period of RF is 84ps (6GHz)

The resonator field theory is described by the equation

$$\frac{dU_E}{d\tau} = -\frac{\omega}{Q}U_E + P_{out}, \tag{44}$$

where P_{out} is the energy output from the bunch and U_E is the electric energy in the cavity. The value of P_{out} depends on the behavior of the individual electrons as they move across the gap which in turn depends on the gap voltage and field profile. The axial electric field is only assumed by sinusoidal shape as $E(t_y) = E_0 \sin(\omega t_y)$.
Define

$$\left\langle f(t_y) \right\rangle \equiv \frac{\omega}{2\pi}\int_0^{\frac{2\pi}{\omega}} f(t_y)dt_y. \tag{45}$$

Then, the time-averaged output power becomes

$$\begin{aligned} \left\langle P_{out} \right\rangle &= \left\langle \int_0^d \rho E v dz \right\rangle = \left\langle \int_0^d J_{peak} E_0 Max\left(\sin^2(\omega t_y), 0\right) dz \right\rangle \\ &= \frac{\omega}{2\pi}\int_0^{\frac{2\pi}{\omega}}\int_0^d J_{peak} E_0 \sin^2(\omega t_y)\, dz dt_y = \frac{J_{peak} E_0 d}{4}. \end{aligned} \tag{46}$$

Because $E = 0$ when there are non electron charges, from the Maxwell's equation set,

$$\left\langle \frac{\omega}{Q} U_E \right\rangle = \frac{\varepsilon\omega}{2Q} \left\langle \int_0^d E_0^2 Max\left(\sin\left(\omega t_y\right), 0\right)^2 dz \right\rangle \cong \frac{\varepsilon\omega}{2Q} \frac{E_0^2}{2} \left\langle \int_0^d \sin^2\left(\omega t_y\right) dz \right\rangle$$
$$= \frac{\varepsilon\omega E_0^2}{4Q} \left\langle \int_0^d \sin^2\left(\omega t_y\right) dz \right\rangle = \frac{\varepsilon\omega E_0^2 d}{4Q} \left\langle \sin^2\left(\omega t_y\right) \right\rangle = \frac{\varepsilon\omega E_0^2 d}{8Q}. \tag{47}$$

Since

$$\left\langle P_{out} \right\rangle = \left\langle \frac{\omega}{Q} U_E \right\rangle \tag{48}$$

at steady state, we have

$$E_0 = \frac{2QJ_{peak}}{\varepsilon\omega}. \tag{49}$$

Therefore, the efficiency becomes that

$$\eta = \frac{\left\langle P_{out} \right\rangle}{\left\langle J \right\rangle V} = \frac{\frac{J_{peak} E_0 d}{4}}{\frac{J_{peak}}{\pi} V} = \frac{\pi E_{0d}}{4V} = \frac{\pi Q J_{peak} d}{2\varepsilon\omega V}. \tag{50}$$

As an example,

$$\begin{aligned} &\varepsilon = 8.85\times10^{-12} F/m, \\ &\omega = 2\pi\times10^9 / \sec, \\ &d = 0.4\times10^{-3} m, \\ &Q = 37 \end{aligned} \tag{51}$$

give us the followings

$$J_{peak} = \frac{3}{\pi\{(9.4\times10^{-3})^2 - (5.7\times10^{-3})^2\}} = 1.71[A/cm^2], \tag{52}$$

where $V = 2000 volts$, $e = 1.6\times10^{-19} C$, and $m = 9.1\times10^{-31} kg$.
Therefore,

$$\eta = \frac{\pi Q J_{peak} d}{2\varepsilon\omega V} = 0.60 \tag{53}$$

and

$$E_0 = \frac{2QJ_{peak}}{\varepsilon\omega} = 3.8\times10^6 V/m. \tag{54}$$

In the previous example, we have seen that the tube reveals 67% efficiency and the electric field in the gap region was $4\times10^9 V/m$. This result of the numerical analysis is well matched with the above theoretical calculations.

On the other hand, we can compare MAGIC analysis with analytical calculation as can be seen Fig. 12 which shows efficiency vs. peak current density by MAGIC PIC simulation and analytical calculation. The slope of the line fitted with the results from MAGIC analysis shows 0.266.
From the analytical equation of efficiency, we can get the slope of the line, m, as the followings,

$$m = \frac{\eta}{J_{peak}} = \frac{\pi Q d}{2\varepsilon\omega V} = 0.348 cm^2 / A. \tag{55}$$

Analytical calculation says the slope of the line be 0.348. MAGIC and analytical equation reveal that as we increase the current density, the efficiency of the tube also increases.

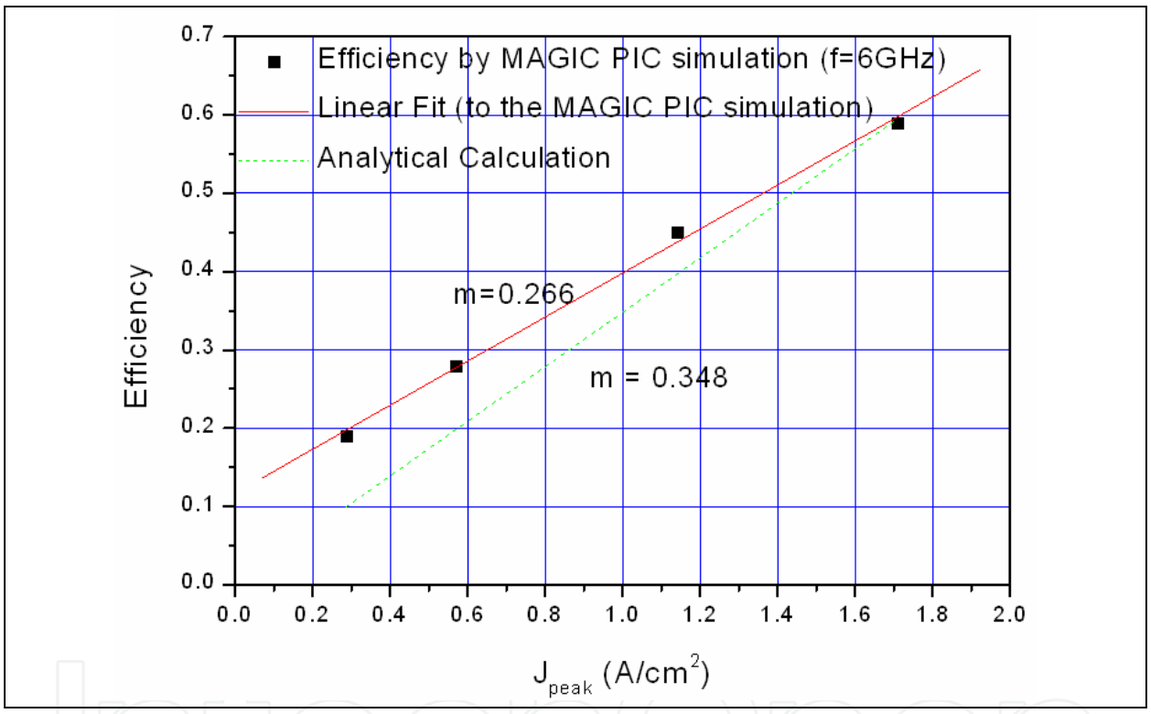

Fig. 12. Efficiency vs. peak current density. Square dots are results from MAGIC simulation. Solid line is line fit with the results. Dotted line is analytical calculation. The slope of the solid line, line fit with the MAGIC results, is 0.266 and that of dotted line from analytical calculation is 0.348

4. Cavity design for the uniform atmospheric microwave plasma source

The atmospheric-pressure microwave-sustained plasma has aroused considerable interest for many application areas. The advantages of this plasma are electrode-less operation and efficient microwave-to-plasma coupling. It has the characteristics of high plasma density ($\approx 10^{13} / cm^{-3}$) and efficient energy conversion from microwaves to the discharged plasma which is high-efficient plasma discharge (~80%). An atmospheric-pressure microwave-sustained plasma can be formed in a rectangular resonant cavity, a waveguide, or a surface-

effect system. This plasma has been widely used in the laboratory spectroscopic analysis, continuous emissions monitoring in the field, commercial processing, and other environmental applications.

Atmospheric-pressure microwave plasma sources consist of a magnetron as a microwave source, an isolator to isolate the magnetron from the harmful reflected microwave, a directional coupler to monitor the reflected microwave power, a 3-stub tuner to match impedance from the magnetron to that from the plasma generator, and a plasma generator through which gases pass and are discharged by the injected microwave. The plasma in the discharge generator is sustained in a fused quartz tube which penetrates perpendicularly through the wide walls of a tapered and shorted WR-284 waveguide.

The plasma's cross-sectional area of the atmospheric-pressure microwave plasma source is limited by the quartz tube's diameter, which is also limited by the maximum intensity of the electric field profile sustainable by the injected microwave and the shorted waveguide structure, as shown in the Fig. 13. The diameter of the quartz tube is set around 30 mm to maintain a dischargeable electric field intensity in the discharge area. If the diameter of the quartz tube becomes much larger than that, no discharge occurs. This is the main reason that the cross-sectional area cannot be extended more widely in the atmospheric-pressure microwave-sustained plasma source.

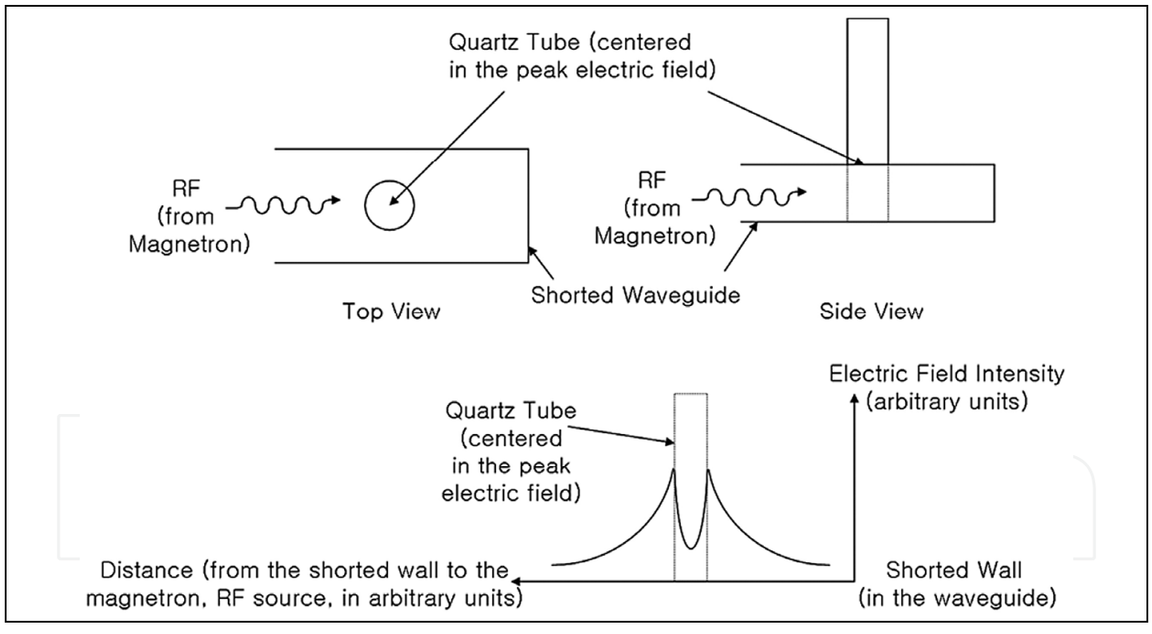

Fig. 13. Schematic illustrations of the atmospheric pressure microwave plasma source using a quartz tube located a quarter wavelength from the end of the shorted waveguide to maintain a high electric field intensity to discharge the passing- gases to generate a plasma efficiently

Here is an example of a rectangular reentrant resonator, a single ridge cavity, to overcome this size-limited plasma discharge in an atmospheric microwave-sustained plasma source. The box-type 915 MHz reentrant resonator has gridded walls on both sides of the gap so that the plasma gases pass thorough the grid holes and are discharged by the induced

electric gap field due to the injected microwave energy. As we have studied in last section, it could be calculated analytically the cavity design formula by using lumped-circuit approximation, then, we performed a RF simulation by using the HFSS (High Frequency Structure Simulator) code. The designed plasma cross-sectional area is 810 mm x5 mm. The cavity has a fundamental TE_{10}-like mode to discharge gases uniformly between the gridded walls and has a 915 MHz resonant frequency. This large cross-sectional area plasma torch can be effectively used in commercial processing and other environmental applications.

4.1 Numerical analysis of the plasma source rectangular cavity

A reentrant cavity in cylindrical symmetry has been widely used in vacuum tubes such as klystrodes and klystrons. However, in order to keep the resonant frequency constant whatever the cavity lengths for atmospheric microwave plasma torch, it would be better to consider a rectangular reentrant cavity, as shown in Fig. 14. The resonant frequency of the cavity for the atmospheric microwave plasma source has a fundamental TE_{10}-like mode.

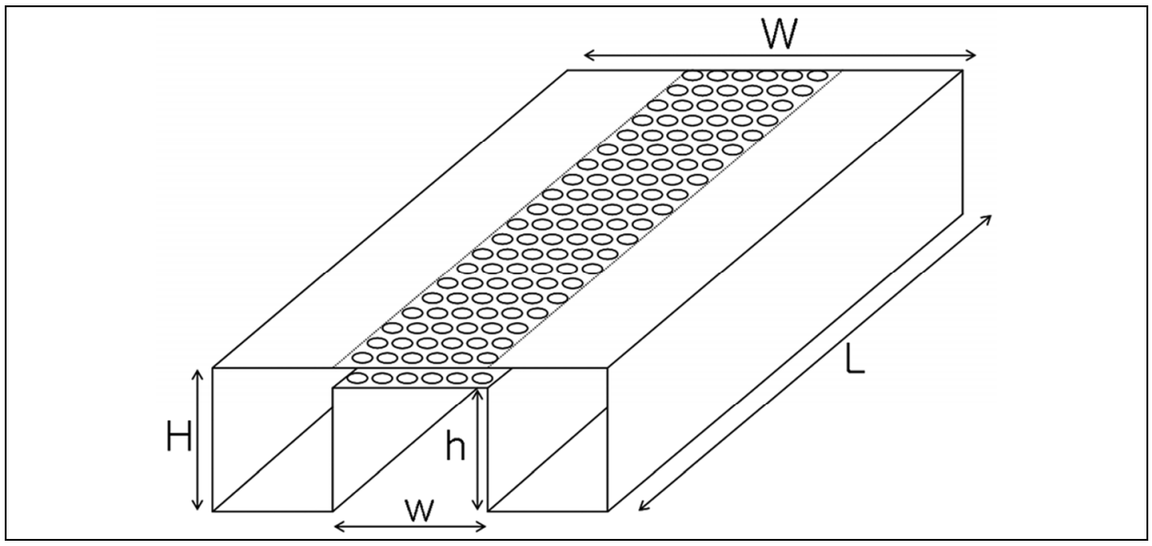

Fig. 14. Schematic of the box-type resonator cavity as a atmospheric pressure microwave plasma source with grids to maintain a high electric field intensity to discharge the passing gases to generate plasma efficiently in the gap region

The gap region between the two gridded walls in the reentrant cavity sustains a high electric field intensity and, thus, easily discharges the gases to the plasma state when it is excited by the microwave energy. With the grid planes surrounding the gap region, the TE_{10}-like mode is the dominant one, and 915 MHz is the cavity's resonant frequency. In the simulation process using the HFSS code, the cavity grids were assumed to be smooth conducting surfaces to design the box-type reentrant cavity.

In this example, the cavity for the microwave plasma source was set to be resonated at 915 MHz, rather than 2.45 GHz, so as to have a much larger cross-sectional plasma area. Its design, setting a cavity to 915 MHz, is based on the design formula obtained by using a theoretical calculation based on the lumped-circuit approximation for the cavity. Then, we used a simulation tool, the HFSS code, to check the cavity frequency.

From Gauss' law, the equivalent capacitance value of the reentrant cavity for a TE_{10}-like mode is

$$C = \frac{Q}{V} = \frac{Q}{E_{\perp}(H-h)} = \frac{\varepsilon_0 L w}{H-h}, \tag{56}$$

where Q, V, and $E_{\perp}$ are the stored electric charges on the grid surfaces, the electric voltage difference, and the perpendicular electric field intensity between the opposite grid surfaces respectively, and w, H, and h are designated dimensional parameters, as shown in Fig. 14. From Ampere's law, the equivalent inductance value of the reentrant cavity for a TE_{10}-like mode can be expressed as follows. Since the magnetic field flux density in the cavity is $B = \mu_0 I / 2L$, and since the total magnetic flux in the box-type reentrant cavity is $\Phi = BH(W-w)$, from the inductance definition,

$$L = \frac{\mu_0 H(W-w)}{4L} \quad . \tag{57}$$

Therefore, the cavity resonant frequency is given by

$$f = \frac{c}{\pi}\sqrt{\frac{H-h}{Hw(W-w)}} \, . \tag{58}$$

This resonant frequency formula shows that the resonant frequency is independent of the cavity length L, which means that if we extrude the plasma through this grid planes, the plasma's cross-sectional area can be uniformly extended as much as we want without any influence on the cavity resonant frequency. However, because we use an available microwave source, which has a limited RF power, to discharge the gases, the cavity length cannot be extended to an unlimited extent. We will discuss this relationship between the consumption RF power and the cavity length in the next paragraph.

Since we have a theoretically-approximated expression for the design parameters, we should use this formula to pick up the initial design parameters to get detailed parameters for the resonator reentrant cavity as a plasma source. Then we should investigate the RF characteristics using the design tool, HFSS.

The energy stored in the gap region can be expressed as

$$U = \frac{1}{2} C V^2 \quad , \tag{59}$$

where C and V are the equivalent capacitance value of the cavity and the induced gap peak voltage between the grid planes, respectively. If we assume that all of this stored energy can be delivered to the gas discharge reaction process to generate the plasma, the microwave power consumption can be expressed as

$$P = \frac{1}{2} f C V^2 = \frac{L V^2}{2\pi}\sqrt{\frac{\varepsilon_0 \omega}{\mu_0 H(H-h)(W-w)}} \, . \tag{60}$$

In other words, the cavity length for the atmospheric-pressure microwave-sustained plasma source is

$$L = \frac{2000\pi P}{V^2}\sqrt{\frac{\mu_0 H(H-h)(W-w)}{w}}\,, \tag{61}$$

where V is in kV, P is in kW, and the dimensional parameters, L, H, h, W, and w, are in mm units in this formula.

Fig. 15 and Fig. 16. show a rectangular cavity design example using one of the available magnetrons, 915 MHz, 60 kW, as a RF source, and the geometrical parameters to $H = 29mm$, $H - h = 1mm$, and $W = 80mm$. Furthermore, if the gap voltage is the upper-limit RF air breakdown voltage, that is, the DC breakdown voltage for air at the level of $33kV/cm$ at atmospheric pressure, the cavity length is limited by $810mm$ for self discharge. In this case, the plasma's cross-sectional area is uniformly distributed within $810mm \times 5mm$, i.e., $w = 5mm$.

This uniformly distributed plasma area is $810mm \times 5mm$, which is much larger than the areas of the conventional atmospheric-pressure microwave-sustained plasma sources. This large-sized microwave plasma at atmospheric pressure can be used in commercial processing and other environmental applications area.

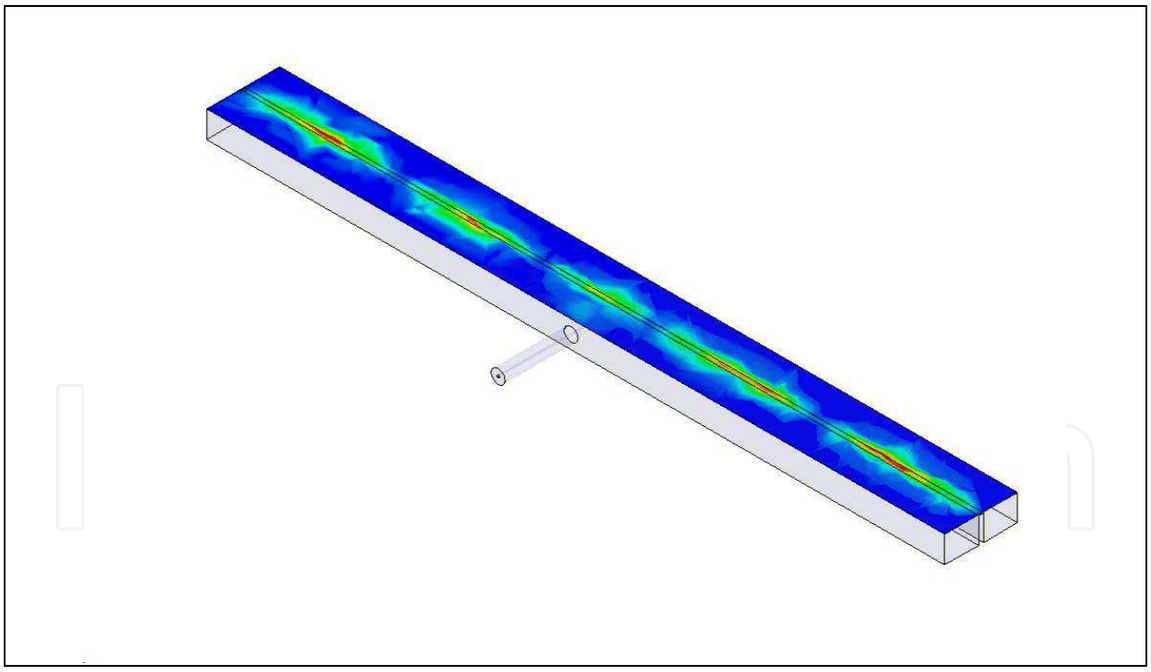

Fig. 15. Electric field intensity profile of the TE10-like mode from the HFSS simulation on the mid-plane between the grid surfaces in the gap region. Both ends are shorted walls, and the electric field profiles are distributed within $810mm \times 5mm$ in the gap region. Microwave energy is feeding through the coaxial coupler to the cavity. If we use a pair of these cavities in parallel, the crest of one will compensate for the other's trough electric field intensity areas, which could result in a uniform microwave plasma source

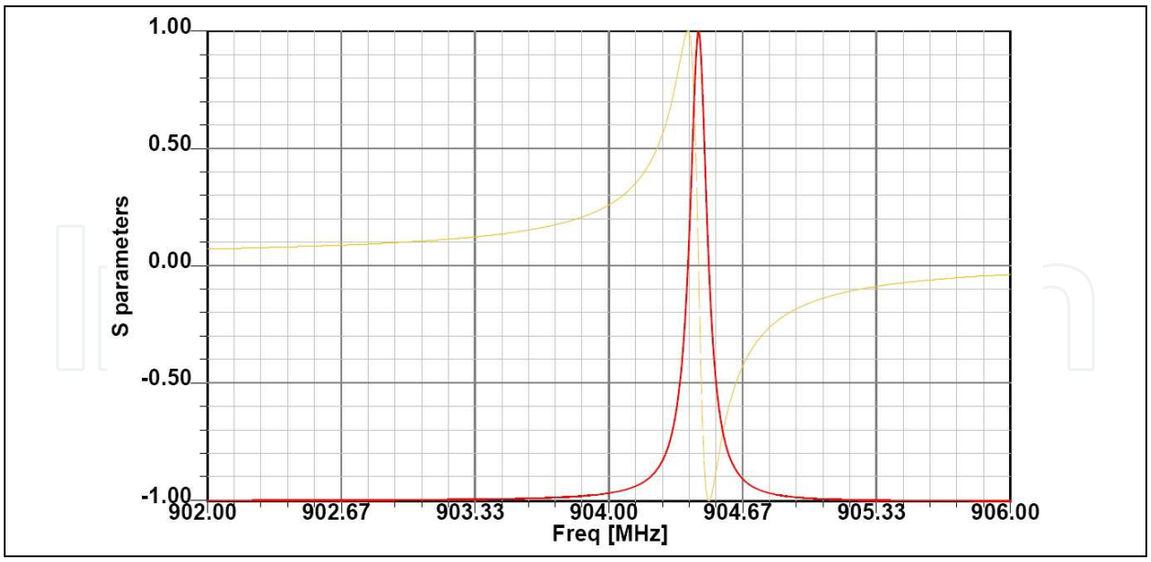

Fig. 16. Scattering parameters of the box-type reentrant cavity. The solid red and dashed blue lines are the real and imaginary values of S11, respectively. This shows that the cavity has a resonant frequency of 904 MHz and a high Q value of 7400

5. Conclusion

The annular beam cavity design was investigated analytically and simulated using the HFSS and MAGIC PIC codes to find the fine-tuned design parameters and optimum efficiency of the TM_{01}-mode operation in the klystrode with the reentrant interaction cavity. We also studied how to induce the governing efficiency formular for the microwave vacuum tube, klystrode. The efficiency of this exampled annular beam klystrode reveals 67 % at 6.004 GHz. The theoretical calculation anticipated that the efficiency would be 60% and the electric field intensity 4000V/m which is well matched with the results of numerical analysis. This concept could yield an economic sized device comparable to commercial magnetron devices.

A single ridge cavity was designed to show how to design uniform atmospheric microwave plasma source which does not need ignitors for the initial discharge. The single ridge cavity in the shape of resonator was built in the grid structures for the wide cavity torch of atmospheric pressure microwave plasma. This cavity design process has been studied by analytical calculation using lumped circuit approximation and simulation using commercial 3D HFSS code. A self-dischargeable study also has been investigated for the breakdown feasibility in the cavity gap region. These cavities show the uniform electromagnetic wave distribution between the grids through which large-sized microwave plasma could be generated.

6. References

Ansoft Co. (1999). High Frequency Structure Simulator, version 6.0, *Ansoft Co.*, PA, USA, 1999

Burton, A. J.; & Miller, G. F. (1971). The application of integral equation methods to the numerical solution of some exterior boundary-value problems, *Proc. Roy. Soc. Lond.*, A. 323, 201 1971

Curnow, H. J. (1965). A General Equivalent Circuit for Coupled-Cavity Slowe-Wave Structures, *IEEE Transactions on Microwave Theory and Techniques*, Vol. MTT-13, No. 5, 671, Sep. 1965

Dai, F. & Omar, A. S. (1993). Field-analysis model for predicting dispersion property of coupled-cavity circuits, *IEEE MTT-S Digest*, 901 1993

Fallgatter, K.; Svoboda, V. & Winefordner, J.D. (1971). Physical and analytical aspects of a microwave excited plasma, *Applied Spectrocopy*, 25, no.3, 347 1971

Fujisawa, K. Fujisawa (1951). Theory of slotted cylindrical cavities with transverse electric field, *Tech. Reps. Osaka Univ.*, Vol. 1, 69, 1951

Fujisawa,. K. (1958). General treatment of klystron resonant cavities, *IRE Trans.*, MTT-6, 344, Oct. 1958

Gilmour, Jr.,A.S. (1986) Microwave Tube, *Artech House*, Chap. 15 1986

Goplen, B.; Ludeking, L.; Nguyen, K. & Warren, G. (1990). Design of an 850MHz klystrode, *International Electron Devices Meeting*, 889 1990

Goplen, B.; Ludeking, L.; Smithe, D. & Warren, G. (1994). MAGIC User's Manual, Rep. MRC/WDC-R-326, *Mission Res. Corp., Newington, VA*, 1994

Hamilton, D. R.; Knipp, J. K. & Kuper, J. B. Horner (1966). Klystrons and Microwave Triodes, *Dover Pub., New York*, 1966

Hansen, W. W. (1938). A type of electrical resonator, *Journal of Applied Physics*, Vol. 9, 654, Oct. 1938

HeBe, Z. (1997). The cold quality Qcold for magnicon on resonator in the rotating TMn10 mode, *International Journal of Infrared and Millimeter Waves*, Vol. 18, No. 2, 437 1997

Kim, Hyoung S. & Uhm, Han S. (2001). Analytical Calculations and Comparison with Numerical Data for Annular Klystrode, *IEEE Transactions on Plasma Science*, Vol. 29, Issue 6, pp. 875-880, Dec. 2001

Kim, Hyoung Suk & Ahn, Saeyoung (2000). Numerical Analysis of C-band Klystrode with Annular Electron Beam, *International Journal of Infrared and Millimeter Waves*, Vol. 21, No. 1, pp. 11-20, Jan. 2000

Kleinman, R. E. & Roach, G. F. (1974). Boundary Integral equations for the three-dimensional Helmholtz equation, *SIAM Review*, Vol. 16, No. 2, 214, April 1974

Lee, S. W.; Kang, H. J.; Kim, H. S. & Hum, H. S. (2009). Numerical Design of the Cavity for the Uniform Atmospheric Microwave Plasma Source, *Journal of Korean Physical Society*, Vol. 54, No. 6, pp. 2297-2301, June 2009

Liao, Samuel Y. (1990). Microwave Devices & Circuits, *Prentice Hall*, 1990

Marks, R. B. (1986). Application of the singular function expansion to an integral equation for scattering, *IEEE Transactions on Antennas and Propagation*, Vol. AP-34, No. 5, 725, May 1986

Mcdonald, S. W.; Finn, J. M.; Read, M. E. & Manheimer, W. M. (1986). Boundary integral method for computing eigenfunctions in slotted gyrotron cavities of arbitrary cross-sections, *Int. J. Electronics*, Vol. 61, No. 6, 795, 1986

Pearson, L. W. Pearson, (1984). A Note on the representation of scattered fields as a singularity expansion, *IEEE Transactions on Antennas and Propagation*, Vol. AP-32, No. 5, 520, May 1984

Ramm, A. G. (1982). Mathematical foundations of the singularity and eigenmode expansion methods, *Journal of Mathematical Analysis and Applications*, 86, 562 1982

Riddell, R. J. Jr. (1979). Boundary-Distribution Solution of The Helmholtz Equation for a Region with Corners, *Journal of Computational Physics*, 31, 21 1979

Riekmann, C.; Jostingmeier, A. & Omar, A. S. (1996). Application of the eigenmode transformation technique for the analysis of planar transmission lines, *IEEE MTT-S Digest*, 1023 1996

Samuel Seely, (1950). Electron-Tube Circuits, *McGraw Hill Book Com. Inc., New York*, 1950

Stevenson, A. F. (1948). Theory of slots in rectangular wave-guides, *Journal of Applied Physics,* Vol. 19, 24, Jan. 1948

Tan, J. & Pan, G. (1996). A general functional analysis to dispersive structures, *IEEE MTT-S Digest*, 1027 1996

Tobocman, W. (1984). Calculation of acoustic wave scattering by means of the Helmholtz integral equation. I, *J. Acoust. Soc. Am.*, 76 (2), 599, Aug. 1984

Zander, A.T. & Hieftje, G.M. (1981). Microwave-supported discharges, *Applied Spectroscopy*, 35, no. 4, 357 1981

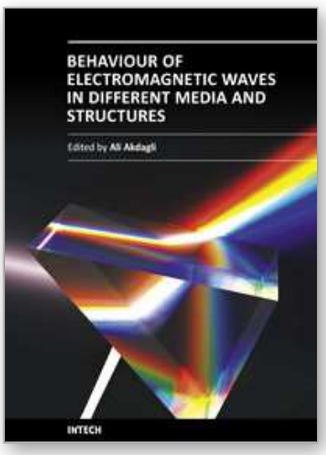

Behaviour of Electromagnetic Waves in Different Media and Structures

Edited by Prof. Ali Akdagli

ISBN 978-953-307-302-6
Hard cover, 440 pages
Publisher InTech
Published online 09, June, 2011
Published in print edition June, 2011

This comprehensive volume thoroughly covers wave propagation behaviors and computational techniques for electromagnetic waves in different complex media. The chapter authors describe powerful and sophisticated analytic and numerical methods to solve their specific electromagnetic problems for complex media and geometries as well. This book will be of interest to electromagnetics and microwave engineers, physicists and scientists.

InTech Europe
University Campus STeP Ri
Slavka Krautzeka 83/A
51000 Rijeka, Croatia
Phone: +385 (51) 770 447
Fax: +385 (51) 686 166
www.intechopen.com

InTech China
Unit 405, Office Block, Hotel Equatorial Shanghai
No.65, Yan An Road (West), Shanghai, 200040, China
中国上海市延安西路65号上海国际贵都大饭店办公楼405单元
Phone: +86-21-62489820
Fax: +86-21-62489821

IntechOpen